nature geoscience

Supplementary information

https://doi.org/10.1038/s41561-026-02067-1

Dense iron oxyhydroxides as possible reservoirs of water under deep mantle conditions

In the format provided by the authors and unedited

Supplementary Information

Contents of this file

Table S1. Experimental conditions and results summary.

Run#	Starting material	P_{300K} (GPa)	T(K)	P gauge	Phase	Beamline	Remarks
PdGlass-S1	peridotite glass + h-SiO_2 + Au	78(1)	2,700(250)	Au	Fe7 + Bdm + Fp + Fe_7C_3 + Ct	ID15B, ESRF	SXRD; LH at ID14, ESRF.
Fs40-Bdm-S1	opx + h-SiO_2+ Ne	82(1)	2,600(200)	Ne	Fe5 + Fe7 + Bdm + Ct	ID15B, ESRF	SXRD; LH at HPSTAR
Fs40-Bdm-P1	opx + h-SiO_2 + Ne	82(1)	2,500-2,800(250)	Ne	Fe5 + Fe7 + Bdm + Ct	P02.2, DESY;	PXRD; *In-situ* LH experiments were performed on a fresh area at P02.2, DESY
Fs40-Bdm-P2	opx + h-SiO_2 +KCl	82(1)	2,400(150)	KCl	Fe5 + Bdm + Ct	15U1a, SSRF	PXRD; LH at HPSTAR; STEM-EDS
WH-S1	wollastonite + hematite	100(1)	2,500(200)	Diamond Raman	Fe5 + Dmv + Fe_3C + Fe_7C_3	ID11, ESRF	SXRD; LH at ID14, ESRF
Fs40-pPv-S1	opx + h-SiO_2+ Ne	114(1)	2,500(200)	Ne	Fe5+ pPv + sft + Fe_7C_3	ID15B, ESRF	SXRD, LH at HPSTAR

FeO2H-S1	α-FeO_2H goethite + Ne	170(1)	2,500(200)	Ne	Fe7 + Fe_3O_4	ID11, ESRF	SXRD, LH at BGI
h-Fe2O3-S1	Fe_2O_3 hematite + Ne[a]	170(1)	2,500(200)	Ne	Fe7 + Fe_3O_4	ID11, ESRF	SXRD, LH at BGI
h-FeO-S1	FeO wüstite + Ar[a]	198(1)	2,700(200)	Ar	Fe7	ID11, ESRF	SXRD; LH at ID14, ESRF

PXRD, powder X-ray diffraction; SXRD, single-crystal X-ray diffraction; LH, laser-heating; RT, room temperature; Fe5, hexagonal $Fe_5O_{12}H_x$ phase; Fe7, hexagonal $Fe_7O_{12}H_x$ phase; opx, $(Mg_{0.6}Fe_{0.4})SiO_3$ orthopyroxene; h-SiO_2, hydrated silica gel; Bdm, bridgmanite; pPv, post-perovskite; Fp, ferropericlase; Dvm, Davemaoite ($CaSiO_3$ perovskite); Ct, $CaCl_2$-type silica; sft, seifertite. Numbers in parentheses indicate uncertainty.

Table S2. Crystal structure, data collection and refinement details of $Fe_5O_{12}H_x$ (Nominal chemical composition is $Fe_{2.5}O_6H_x$ per unit cell) at selected pressures.

CSD Number	2500657	2500658	2500659
Crystal data			
Chemical formula	$Fe_{2.417}O_6H_x$	$Fe_{2.596}O_6H_x$	$Fe_{2.54}O_6H_x$
M_r	231.16	240.65	237.86
Crystal system, space group	Hexagonal, $P6_3/m$	Hexagonal, $P6_3/m$	Hexagonal, $P6_3/m$
Temperature (K)	298	298	298
Pressure (GPa)	82(1)	100(1)	114(1)
a, c (Å)	5.2005(10), 2.8197(9)	5.0960(11), 2.8490(13)	5.0963(9), 2.8113(3)
V (Å^3)	66.04(3)	64.07(4)	63.23(2)
Z	1	1	1
Radiation type	Synchrotron, λ = 0.4099 Å	Synchrotron, λ = 0.2846 Å	Synchrotron, λ = 0.4099 Å
μ (mm^{-1})	2.82	1.15	3.09
Crystal size (mm)	0.001×0.001×0.001	0.001×0.001×0.001	0.001×0.001×0.001
Data collection			
Diffractometer	ESRF ID15b, EIGER2 X 9M CdTe detector	ESRF ID11, Dectris Eiger2 X CdTe 4M	ESRF ID15b, EIGER2 X 9M CdTe detector
No. of measured, independent and observed [$I > 2\sigma(I)$] reflections	51, 34, 29	277, 127, 111	72, 38, 34
R_{int}	0.086	0.039	0.027
$(\sin\theta/\lambda)_{max}$ (Å^{-1})	0.816	1.107	0.747
Refinement			
$R[F^2 > 2\sigma(F^2)]$, $wR(F^2)$, S	0.054, 0.117, 1.41	0.075, 0.189, 1.11	0.064, 0.163, 1.24
No. of reflections	34	127	38
No. of parameters	11	12	9
$\Delta\rho_{max}$, $\Delta\rho_{min}$ (e Å^{-3})	0.99, -1.20	2.16, -2.17	0.98, -1.24
Wyckoff Site	Fe1: 2*c* Fe2: 2*b* Fe3: 2*a* O1: 6*h*	Fe1: 2*c* Fe2: 2*b* Fe3: 2*a* O1: 6*h*	Fe1: 2*c* Fe2: 2*b* Fe3: 2*a* O1: 6*h*
Occupancy	Fe1: 1 Fe2: 0.136(14) Fe3: 0.073(16) O1: 1	Fe1: 1 Fe2: 0.146(18) Fe3: 0.15(3) O1: 1	Fe1: 1 Fe2: 0.20(3) Fe3: 0.069(18) O1: 1

Fractional atomic coordinates (x y z)	Fe1: 1/3 2/3 1/4 Fe2: 0 0 0 Fe3: 0 0 1/4 O1: 0.356(8) 0.036(7) 1/4	Fe1: 1/3 2/3 1/4 Fe2: 0 0 0 Fe3: 0 0 1/4 O1: 0.080(4) 0.386(3) 1/4	Fe1: 1/3 2/3 1/4 Fe2: 0 0 0 Fe3: 0 0 1/4 O1: 0.068(9) 0.375(7) 1/4
U_{iso} (Å^2)	Fe1: 0.0062(12) Fe2: 0.0062(12) Fe3: 0.0062(12) O1: 0.073(15)	Fe1: 0.0051(4) Fe2: 0.013(3) Fe3: 0.032(8) O1: 0.049(4)	Fe1: 0.0084(17) Fe2: 0.037(9) Fe3: 0.037(4) O1: 0.064(5)

14

Table S3. Crystal structure, data collection and refinement details of $Fe_7O_{12}H_x$ at selected pressures.

CSD Number	2500660	2500661
Crystal data		
Chemical formula	$Fe_{7.41}O_{12}H_x$	$Fe_{7.159}O_{12}H_x$
M_r	605.85	591.89
Crystal system, space group	Hexagonal, $P6_3/m$	Hexagonal, $P6_3/m$
Temperature (K)	298	298
Pressure (GPa)	170(1)	198(1)
a, c (Å)	7.2784(15), 2.6688(6)	7.173(3), 2.772(2)
V (Å^3)	122.44(6)	123.49(13)
Z	1	1
Radiation type	Synchrotron, λ = 0.2846 Å	Synchrotron, λ = 0.2846 Å
μ (mm^{-1})	1.69	1.63
Crystal size (mm)	0.001×0.001×0.001	0.001×0.001×0.001
Data collection		
Diffractometer	ESRF ID11, Dectris Eiger2 X CdTe 4M	ESRF ID11, Dectris Eiger2 X CdTe 4M
No. of measured, independent and observed [$I > 2\sigma(I)$] reflections	581, 267, 188	304, 129, 86
R_{int}	0.059	0.063
$(\sin\theta/\lambda)_{max}$ (Å^{-1})	1.100	0.711
Refinement		
$R[F^2 > 2\sigma(F^2)]$, $wR(F^2)$, S	0.076, 0.228, 1.09	0.073, 0.203, 1.10
No. of reflections	267	129
No. of parameters	25	22
$\Delta\rho_{max}$, $\Delta\rho_{min}$ (e Å^{-3})	2.47, -2.41	1.48, -2.40
Wyckoff Site	Fe1: 6*h* Fe2: 2*b* Fe3: 2*a* O1: 6*h* O2: 6*h*	Fe1: 6*h* Fe2: 2*b* Fe3: 2*a* O1: 6*h* O2: 6*h*
Occupancy	Fe1: 1 Fe2: 0.45(4) Fe3: 0.25(5) O1: 1 O2: 1	Fe1: 1 Fe2: 0.415(19) Fe3: 0.164(12) O1: 1 O2: 1

Fractional atomic coordinates (x y z)	Fe1: 0.4417(2) 0.1647(2) 1/4 Fe2: 0 0 0 Fe3: 0 0 1/4 O1: 0.2270(18) 0.241(2) 1/4 O2: 0.1241(14) 0.5149(14) 1/4	Fe1: 0.4447(5) 0.1692(5) 1/4 Fe2: 0 0 0 Fe3: 0 0 1/4 O1: 0.230(6) 0.246(5) 1/4 O2: 0.140(4) 0.525(4) 1/4
U_{iso} (Å^2)	Fe1: 0.0112(4) Fe2: 0.017(3) Fe3: 0.061(8) O1: 0.035(2) O2: 0.0273(19)	Fe1: 0.0203(11) Fe2: 0.005(3) Fe3: 0.005(3) O1: 0.096(12) O2: 0.082(9)

17

Table S4. Crystal structure, data collection and refinement details of one coexisting Fe-bearing bridgmanite crystal at 100 GPa.

Crystal data	
Chemical formula	$Fe_{0.065}Mg_{0.935}SiO_3$
M_r	102.4
Crystal system, space group	Orthorhombic, *Pnma*
Temperature (K)	298
Pressure (GPa)	100(1)
a, c (Å)	4.642(6), 6.408(3), 4.416(3)
V (Å^3)	131.4 (2)
Z	4
Radiation type	Synchrotron, λ = 0.4099 Å
μ (mm^{-1})	0.52
Crystal size (mm)	0.001×0.001×0.001
Data collection	
Diffractometer	ESRF ID15b, EIGER2 X 9M CdTe detector
No. of measured, independent and observed [$I > 2\sigma(I)$] reflections	187, 102, 89
R_{int}	0.015
Refinement	
$(\sin\theta/\lambda)_{max}$ (Å^{-1})	1.100
$R[F^2 > 2\sigma(F^2)]$, $wR(F^2)$, S	0.040, 0.050, 3.71
No. of reflections	102
No. of parameters	16
$\Delta\rho_{max}$, $\Delta\rho_{min}$ (e Å^{-3})	2.47, -2.41
Wyckoff Site	Mg1: 4*c* Fe1: 4*c* Si1: 4a O1: 4*c* O2: 8*d*
Occupancy	Mg1: 0.935(10) Fe1: 0.065(10) Si1: 1 O1: 1 O2: 1
Fractional atomic coordinates (x y z)	Mg1: 0.4297(7) 1/4 0.0215(5) Fe1: 0.4297(7) 1/4 0.0215(5) Si1: 0 0 0 O1: 0.5335(14) 1/4 0.6117(13) O2: 0.1961(10) 0.0551(6) 0.3125(8)

20	U_{iso} (Å^2)	Mg1: 0.0089(11) Fe1: 0.0089(11)
21		Si1: 0.0084(6) O1: 0.0110(11)
22		O2: 0.0098(8)

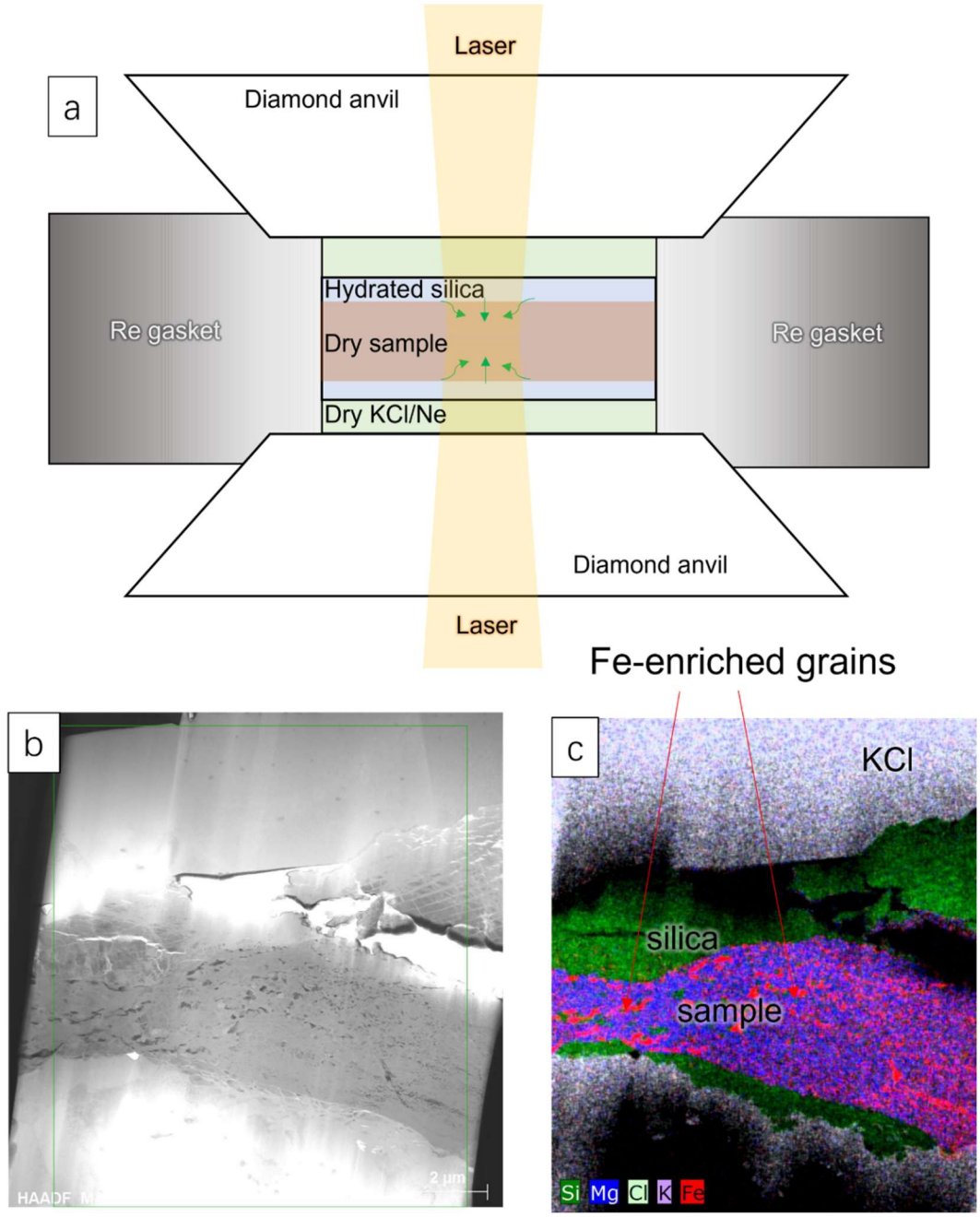

Figure S1. Sample assembly in a laser-heating diamond anvil cell and cross-section of the recovered sample. For the $(Mg_{0.6}Fe_{0.4})SiO_3$ orthopyroxene starting sample, a double sandwich assembly is employed (**a**). The starting sample is firstly sandwiched by hydrated silica gel layers (serving as a water source), which is then placed within KCl or Ne as pressure medium and thermal insulator. The recovered sample is positioned, cut and milled to a TEM-transparent (<100 nm in thickness) film (**b**) and subsequently characterized by STEM-EDS analysis (**c**).

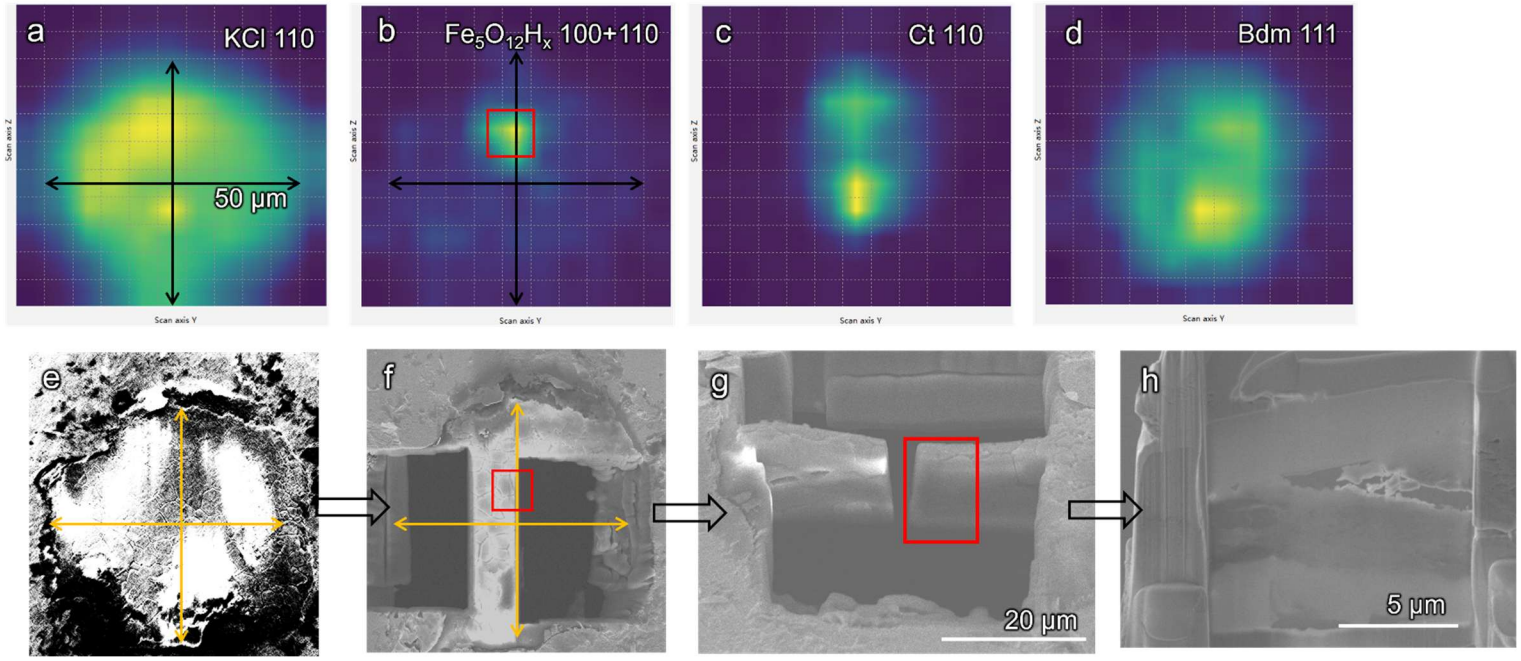

Figure S2. High-pressure XRD map of the phase of interest and corresponding SEM-FIB cutting process of the recovered sample from Run Fs40-Bdm-P2. The XRD maps are constructed based on the intensity contrast of characteristic diffraction peak(s) for individual phases including KCl (**a**), $Fe_5O_{12}H_x$ (**b**), $CaCl_2$-type silica (Ct) (**c**) and bridgmanite (Bdm) (**d**). The SEM image of the recovered sample (**e**) matches high-pressure XRD map of KCl (**a**), indicating that the sample does not distort during the decompression process. Guided by the high-pressure XRD map, the region of the recovered $Fe_5O_{12}H_x$ has been accurately positioned (**e**) and cut, as shown from front view (**f**) and side view (**g**). The positioned sample is ultimately milled to a TEM-transparent (<100 nm in thickness) film (**h**).

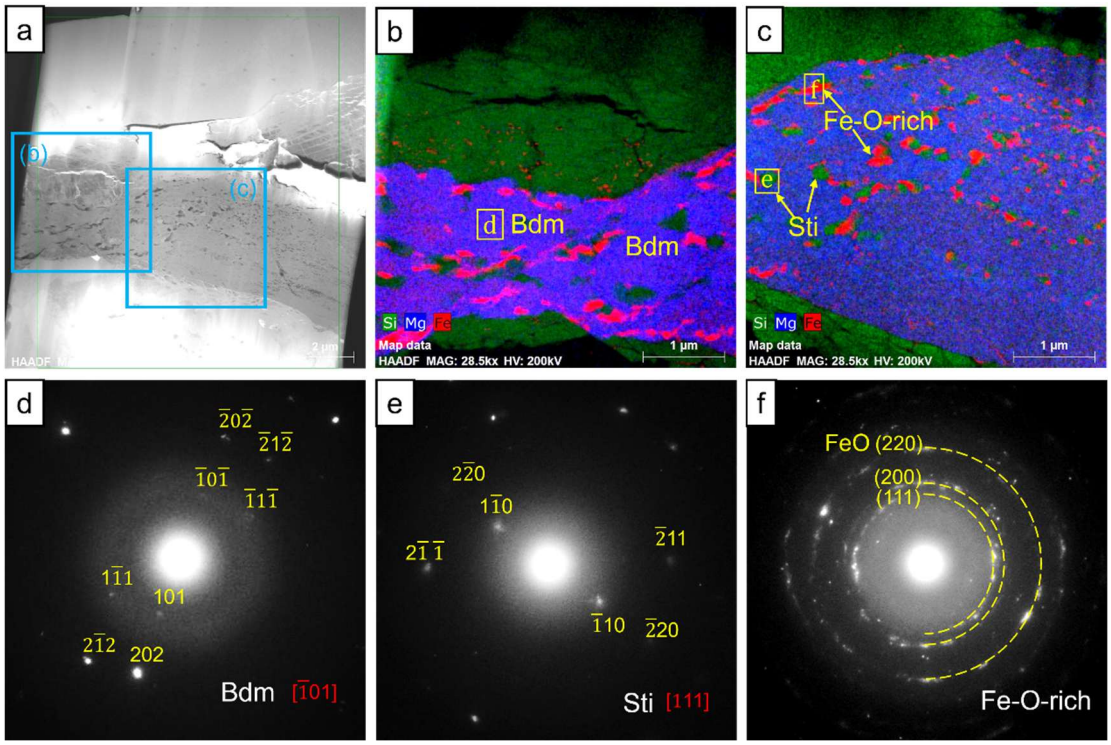

Figure S3. STEM-EDS-SAED analysis of recovered sample from Run Fs40-Bdm-P2. a, High-angle angular dark-field (HAADF) image of the recovered sample. **b,c** EDS elemental maps of the region outlined in **a**, showing silicon (green), magnesium (blue), and iron (red) distributions. **d-f,** Selected-area electron diffraction (SAED) patterns: **d,** silicate phase identified as bridgmanite (Bdm), **e,** silica phase identified as stishovite (sti, recovery product of high-pressure $CaCl_2$-type silica), **f** Fe-O-rich phase assigned to B1-FeO phase. The high-pressure XRD pattern (Fig. 2b in the main text) shows the formation of $Fe_5O_{12}H_x$ phase instead of FeO phase, suggesting that $Fe_5O_{12}H_x$ phase breaks down to FeO phase upon decompression to ambient conditions. Note that our evidence indicates that the previously observed "H-phase" is identical to the $Fe_5O_{12}H_x$ phase observed in this study. They have shown that "H-phase" become amorphous after recovered to ambient conditions. It is possible that recovered amorphous $Fe_5O_{12}H_x$ phase might transform into B1-FeO phase during FIB milling or STEM analysis.